Farnesyl Diphosphate Synthase Inhibitors With Unique Ligand-Binding Geometries

Yi-Liang Liu, Rong Cao, Yang Wang, and Eric Oldfield*

Department of Chemistry, University of Illinois at Urbana–Champaign, Urbana, Illinois 61801, United States

Ⓢ *Supporting Information*

ABSTRACT: Farnesyl diphosphate synthase (FPPS) is an important drug target for bone resorption, cancer, and some infectious diseases. Here, we report five new structures including two having unique bound ligand geometries. The diamidine inhibitor **7** binds to human FPPS close to the homoallylic (S2) and allosteric (S3) sites and extends into a new site, here called S4. With the bisphosphonate inhibitor **8**, two molecules bind to *Trypanosoma brucei* FPPS, one molecule in the allylic site (S1) and the other close to S2, the first observation of two bisphosphonate molecules bound to FPPS. We also report the structures of apo-FPPS from *T. brucei*, together with two more bisphosphonate-bound structures (**2,9**), for purposes of comparison. The diamidine structure is of particular interest because **7** could represent a new lead for lipophilic FPPS inhibitors, while **8** has low micromolar activity against *T. brucei*, the causative agent of human African trypanosomiasis.

KEYWORDS: Farnesyl diphosphate synthase, inhibitor, *T. brucei*, diamidine
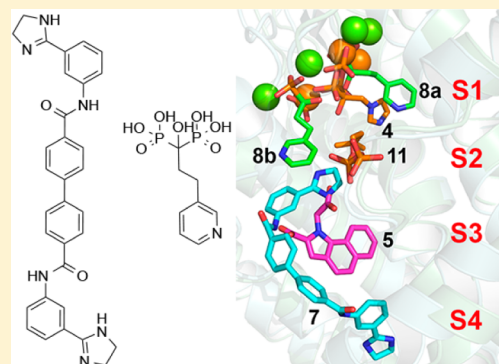
The bisphosphonate class of drugs[1] such as alendronate (**1**), risedronate (**2**), ibandronate (**3**), and zoledronate (**4**) that are used to treat bone resorption diseases (osteoporosis, hypercalcemia due to malignancy, and Paget's disease) function primarily by targeting the enzyme farnesyl diphosphate synthase (FPPS) in osteoclasts.[2,3] They also have other interesting effects including inhibiting tumor cell invasiveness;[4] activating gamma delta T-cells (containing the Vγ2 Vδ2 T-cell receptor) to kill tumor cells and bacteria;[5] they switch tumor-associated macrophages from a tumor promoting (M2) to a tumor-inhibiting (M1) phenotype;[6] and they have activity as antiparasitics.[7,8] There is, therefore, interest in the further development of FPPS inhibitors for use against a broad range of diseases because farnesyl diphosphate (FPP) plays a key role in many different biosynthetic pathways including protein prenylation; glycosylation, bacterial cell wall, quinone, and heme a biosynthesis; as well as in formation of several bacterial virulence factors.[9–12] This interest is reflected in, for example, the recent development of new classes of FPPS inhibitors[13,14] including compounds such as **5** and **6**, these more hydrophobic species being of interest as potential anticancer drug leads that target soft tissues.[13]

Here, we report the results of an investigation into the structures of two FPPS inhibitors that we find have unusual binding modes, not reported previously: the diamidine inhibitor **7** (BPH-1358; NSC50460; *N*-[3-(4,5-dihydro-1*H*-imidazol-2-yl)phenyl]-4-[4-[[3-(4,5-dihydro-1*H*-imidazol-2-yl)phenyl]-carbamoyl]phenyl]benzamide dihydrochloride), bound to human FPPS; and the bisphosphonate inhibitor **8** (BPH-6; NE-58051; 1-hydroxy-1-phosphono-3-(pyridin-3-yl)propyl

phosphonic acid), bound to *Trypanosoma brucei* FPPS. We also report the structures of risedronate **2** and the amino-methylene bisphosphonate **9**, bound to *T. brucei* FPPS (TbFPPS), as well as that of apo TbFPPS, for purposes of comparison. The diamidine **7** is of interest since it has quite potent activity against human FPPS and is hydrophobic, enabling soft tissue penetration, and is not expected to bind to bone mineral. The bisphosphonate **8** is of interest because it has been the topic of a computational investigation into the mechanism of FPPS inhibition;[15] it has activity against the trypanosomatid parasite *Trypanosoma brucei*,[16] and we report here that, as with **7**, **8** has an unusual FPPS binding mode.

The reactions catalyzed by FPPS involve the sequential condensation of the allylic species dimethylallyl diphosphate (DMAPP, **10**) with isopentenyl diphosphate (IPP, **11**) to form geranyl diphosphate (GPP, **12**) and thence farnesyl diphosphate (FPP, **13**), Figure 1. Carbocations are transition state/reactive intermediates,[17] and the side-chains in the most potent bisphosphonate FPPS inhibitors have been proposed to act as carbocation isosteres,[2,9] while the bisphosphonate groups themselves act as diphosphate isosteres. Bisphosphonate inhibitors have all been found to bind to the allylic site S1, as shown in Figure 2, with the two phosphonate groups interacting with a [Mg²⁺]₃ cluster[18] in site S1, the Mg²⁺ in turn being bound to the protein via a cluster of highly conserved Asp residues (a so-called DDXXD motif). The
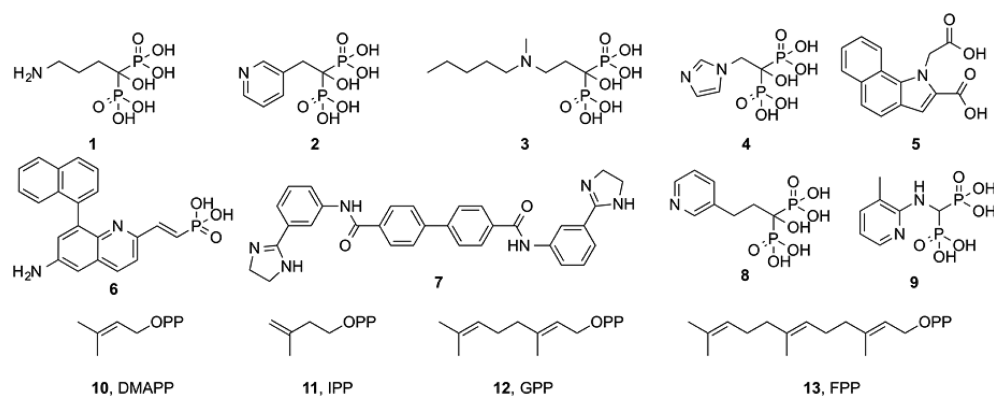
Figure 1. Structures of FPPS inhibitors, substrates, the GPP intermediate, and the FPP product.
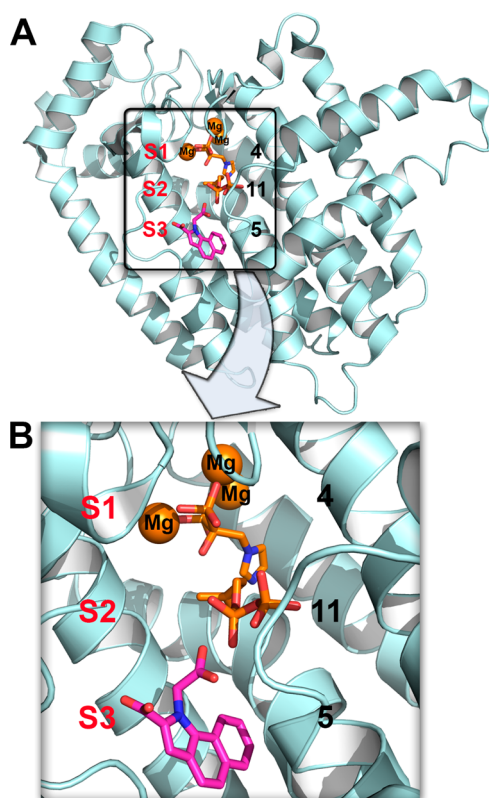

Figure 2. FPPS structures. The structures of **4** + **11** (PDB ID code 2F8Z) and **5** (PDB ID code 3N6K) are shown superimposed. Compound **4** binds in S1, **11** binds in S2, and **5** binds in S3.

homoallylic substrate **11** binds to a second site, S2, with the diphosphate group interacting with Arg/Lys residues. Much larger inhibitors (e.g., the diterpene quinone methide, taxodione, and another quinone methide, arenarone) have also recently been found[19] to bind to the S2 site. A third site, S3, is occupied by the "allosteric" inhibitors developed by Novartis.[13] These are very potent FPPS inhibitors, developed to target tumors in soft tissue,[13] and are located below the **S2** site, in S3, as shown in Figure 2.

We first determined the structure of the FPPS inhibitor **7**, which is of interest since it has an $IC_{50} = 1.8\ \mu M$ against human FPPS[20] under assay conditions where the IC_{50} for the potent FPPS inhibitor **4** (zoledronate) is $0.2\ \mu M$.[20] Since it is also quite lipophilic (clogP = 4.3), **7** could be a new lead for anticancer therapeutics (e.g., against Ras-bearing tumors).[21]

We expressed, purified, and crystallized human FPPS as described previously[19] and obtained crystals with **7** by cocrystallization. Full sample preparation, data acquisition, and data processing details are given in the Supporting Information and Table 1. The basic structure of FPPS is now well-known,[22−25] and as noted above, there are three main inhibitor binding sites, S1−S3, Figure 2. As can be seen in Figure 3A, with the diamidine inhibitor **7**, we find that about one-half of the molecule (three rings) binds to sites S2/S3, while the second half of the molecule (again, three rings) binds to a new site, called here S4, that is outside the S1−S3 site regions reported previously with all other FPPS inhibitors. The 2Fo−Fc electron density is shown contoured at 1σ in Figure 3A, and all rings are well resolved. The discovery map used for initial inhibitor refinement is shown in Figure 3B. Specific ligand−protein interactions are shown in the ligand interaction diagram[26] in Figure 3C and indicate the presence of electrostatic, hydrogen bonding, cation−pi, and hydrophobic (Supporting Information Figure S1A) interactions. In addition, as can be seen in Supporting Information Figure S1B, the central biphenyl ring is quite solvent-exposed. This structure thus represents a new FPPS inhibitor binding mode and may be of interest in the development of more potent compounds.

Next, we investigated the binding of the bisphosphonate **8** to TbFPPS. TbFPPS is a homologue of HsFPPS with 44% identity and 64% similarity overall, and 68% identity and 89% similarity in the active site region. In early work we proposed[2] that bisphosphonates might bind to the FPPS allylic site S1, and this was later found to be the case.[23] It was then suggested[15] that some bisphosphonates might be able to bind to the homoallylic site S2, but to date, no such structures have been reported. As part of our investigation into the structures of FPPS inhibitors, we chose to investigate **8** (BPH-6; NE-58051; 1-hydroxy-1-phosphono-3-(pyridin-3-yl)propyl) phosphonic acid) since this was the subject of the earlier computational docking study.[15] Plus, **8** is of interest because it is an inhibitor of trypanosomatid FPPSs (*Leishmania donovani*, $IC_{50} = 5.4\ \mu M$; *T. brucei* $IC_{50} \approx 33\ \mu M$) and is also active against *T. brucei rhodesiense* with an EC_{50} of $1.7\ \mu M$.[16]

We crystallized *T. brucei* FPPS in its apo form in addition to obtaining cocrystals in the presence of **8**, as well as in the presence of the potent inhibitors **2** (risedronate; $IC_{50} = 300$ nM) and **9** ($IC_{50} = 230$ nM), and solved their structures. Full crystallographic data acquisition and data processing details are given in the Supporting Information and Table 1. The structures of **2** and **9** were as expected, based on all previous FPPS−bisphosphonate structures, the inhibitors binding to S1

Table 1. Data Collection and Refinement Statistics

crystal (PDB ID)	HsFPPS·7 (4RXA)	TbFPPS (4RYP)	TbFPPS·8 (4RXC)	TbFPPS·2 (4RXD)	TbFPPS·9 (4RXE)
Data Collection					
radiation source	21-ID-G	21-ID-G	21-ID-G	21-ID-G	21-ID-G
wavelength (Å)	0.97857	0.97857	0.97857	0.97857	0.97857
space group	$P4_12_12$	$C2$	$C2$	$C2$	$C2$
a (Å)	110.83	134.34	133.01	133.21	134.15
b (Å)	110.83	119,439	120.92	119.55	119.15
c (Å)	77.95	62.04	63.34	62.44	62.82
β (deg)	90	117.18	117.18	111.93	112.24
resolution (Å)[a]	50.0−2.20 (2.24−2.20)	50.0−2.20 (2.28−2.20)	50.0−2.30 (2.38−2.30)	50.0−2.30 (2.38−2.30)	50.0−2.30 (2.38−2.30)
no. of reflections	23767 (1173)	42016 (3334)	37381 (3082)	41878 (2595)	49429 (5184)
completeness (%)	94.4 (95.8)	96.4 (76.7)	97.1 (80.4)	91.0 (56.5)	94.2 (98.4)
R_{merge} (%)	8.2 (75.3)	9.6 (21.7)	12.9 (28.9)	7.3 (42.4)	7.3 (57.6)
$I/s(I)$	30.8 (3.1)	20.9 (4.4)	16.1 (3.0)	10.1 (3.3)	23.9 (3.1)
Refinement					
resolution (Å)[a]	50.0−2.20 (2.25−2.20)	30.0−2.20 (2.28−2.20)	50−2.30 (2.38−2.30)	50.0−2.30 (2.38−2.30)	50.0−2.50 (2.57−2.50)
R_{work} (%)	22.5 (34.3)	18.0 (22.8)	20.0 (24.7)	21.1 (23.7)	19.7 (23.0)
R_{free} (%)	25.9(34.6)	24.1 (27.4)	25.4 (27.4)	25.1 (32.0)	25.5 (33.4)
Geometry Deviations					
bond lengths (Å)	0.018	0.016	0.002	0.010	0.015
bond angles (deg)	0.881	1.669	0.684	1.203	1.826
Mean B-Values (Å²)/Number of Non-H Atoms					
protein atoms	33.8/2659	52.2/5596	43.0/5639	28.3/8549	48.7/5737
compound atoms	63.4/40		51.4/72	18.1/51	34.4/34
PO₄ ions	65.4/5				
Mg ions			46.4/8	19.1/9	41.0/6
water	52.3/104	48.5/176	42.9/153	32.8/484	41.7/158
Ramachandran Plot (%)					
most favored	91.8	91.9	92.2	93.6	90.9
additionally allowed	7.9	7.8	7.8	6.1	9.1
generously allowed	0	0.3	0	0	0
disallowed	0	0	0	0	0

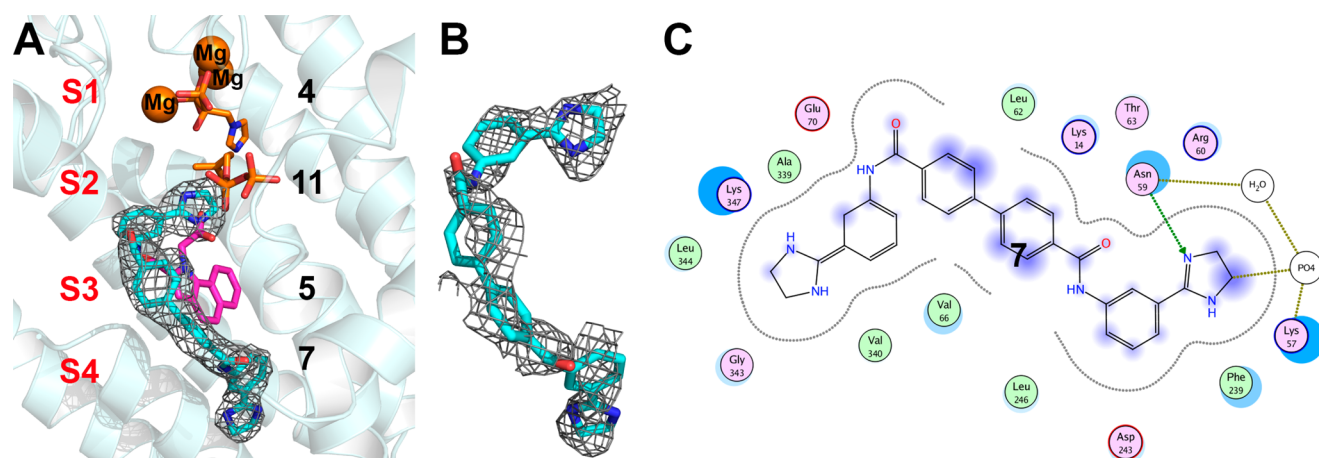[a]Values in parentheses represent the highest resolution shell.

Figure 3. Structure of the diamidine **7** bound to HsFPPS (PDB ID code 4RXA). (A) Compound **7** contoured at 1σ, superimposed on **4**, **5**, and **11** (PDB ID codes 2F8Z and 3N6K) bound to HsFPPS. (B) Discovery map used for initial inhibitor refinement. (C) Ligand interaction diagram for **7** computed by using MOE.[26]

and interacting with 3 Mg²⁺, as shown in Figures 4A,B. Surprisingly, however, we found that the TbFPPS·**8** structure, Figure 4C, contained two bisphosphonates, not just the one found in all other (~50) reported bisphosphonate-containing FPPS structures. In addition, there were four, not three, Mg²⁺.

Electron densities are shown in Figure 4C and ligand−protein interactions in Figure 4D. Figure 4E shows the structure of the complex with **8** superimposed on the structure with risedronate **2** (in S1), in stereo. Clearly, in the structure with **8**, one molecule of **8**, henceforth called **8a**, binds in the allylic site S1
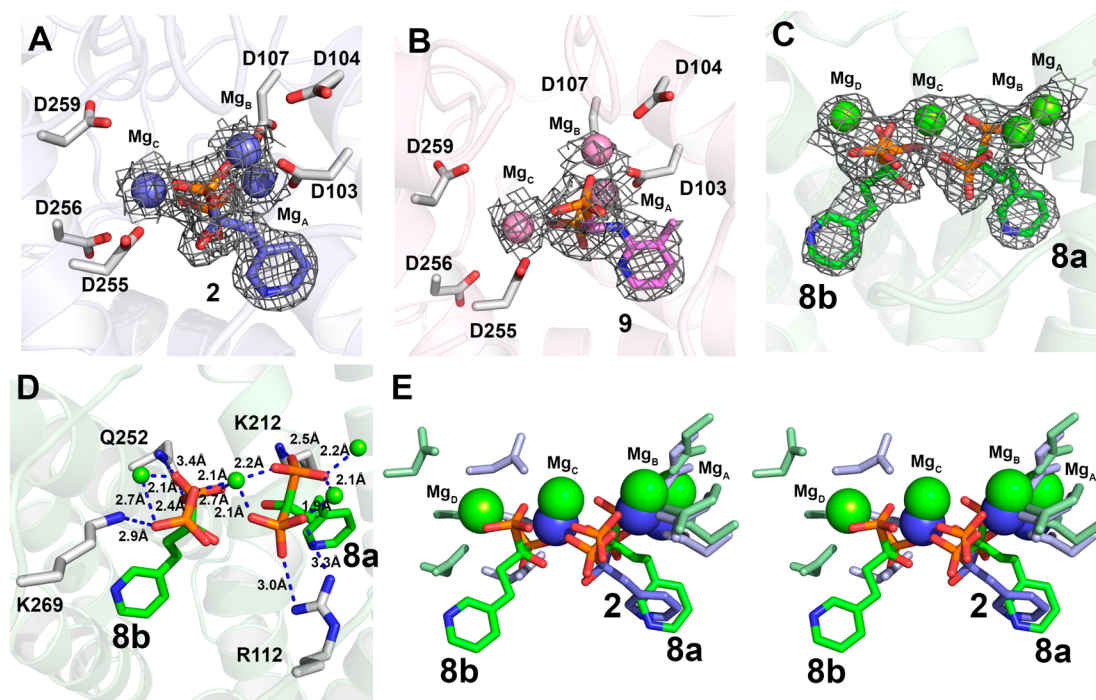
Figure 4. Structures of **2**, **8**, and **9** bound to TbFPPS: (A) **2** (PDB ID code 4RXD); (B) **9** (PDB ID code 4RXE); (C) **8** (PDB ID code 4RXC). (D) Ligand−protein interactions with **8**. (E) Comparison between **2** and **8** TbFPPS structures, in stereo. In panels A−C, the electron density maps are 2Fo−Fc and are contoured at 1σ.

(as do all other bisphosphonates), and in this site, there are interactions with three Mg^{2+} (Mg_A^{2+}, Mg_B^{2+} and Mg_C^{2+}), as shown in Figure 4C,D. These Mg^{2+} are involved in diphosphate removal/carbocation formation. However, as can be seen in Figure 4C,D, there is a fourth Mg^{2+} present in the structure, Mg_D^{2+}, and the second **8** molecule, **8b**, binds with its bisphosphonate groups interacting with Mg_C^{2+} in addition to Mg_D^{2+}, Figure 4C,D. The pyridine side-chain in **8b** is located between the allylic site S1 and the homoallylic site S2 (Figure 5
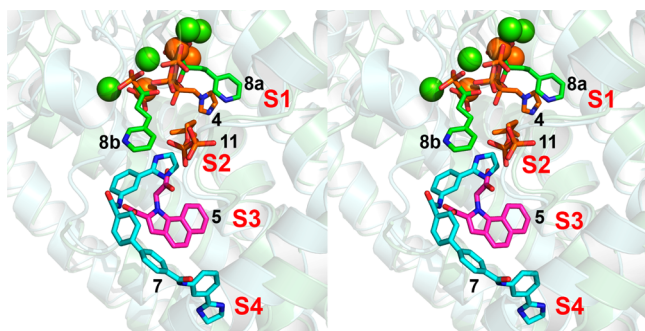

Figure 5. Comparison between the structures of **4**, **5**, **7**, **8**, and **11** bound to FPPS, in stereo.

shows the comparison with zoledronate and **11**), and the pyridine ring in **8b** is more solvent exposed than is found in **8a**, bound to S1. This FPPS structure is interesting because it is the first to contain two bisphosphonate inhibitors bound in the active site; plus, the inhibitor has activity against two trypanosomatid FPPS enzymes as well as against *T. brucei*, but its activity against human FPPS is ∼1000-fold less than is found with more potent bisphosphonates such as risedronate (**2**),[27] and under our assay conditions, **8** did not inhibit human FPPS. We used ITC to investigate the binding of the inhibitor

to *T. brucei* FPPS, and the results are shown in Supporting Information Figure S3. There are two binding sites with similar ΔH and ΔS values, but there is only 19% and 62% occupancy, so there may be stabilization of the two-ligand structure due to lattice packing in the crystalline solid state, or binding of two ligands is just very slow.

When the **8** TbFPPS structure (PDB ID code 4RXC) is compared with the corresponding **2** TbFPPS structure (PDB ID code 4RXD), Supporting Information Figure S2, it is apparent that the α2 helix is closer to the risedronate ligand **2** than it is when in the presence of **8**. There are also rotations of the A and B helices, not observed in the apo-FPPS structure (PDB ID code 4RYP), and the apo-FPPS and **8** structures are very similar. What these results show is that addition of a potent inhibitor causes a closing of the active site pocket, in particular, rotation of helix α2. In the absence of any preincubation with inhibitor, it has been reported that **2** and **8** have basically similar IC_{50} values for human FPPS inhibition (**2**, 82 nM; **8**, 363 nM), but on preincubation, the IC_{50} values are very different (**2**, 0.36 nM; **8**, 78 nM). These results are consistent with the TbFPPS structural results in which the more potent inhibitor **2** causes a closing of the active site that is not seen with **8**, whose structure (even in the presence of two bisphosphonates) is very similar to that of the open, apo-form structure, Figure S2, Supporting Information.

The results we have described above are of interest for two main reasons. First, we find that the novel FPPS inhibitor **7**, a member of a new class of lipophilic FPPS inhibitors, binds to a novel ligand binding site, called here S4, in addition to binding to S2/S3, Figure 5. Such lipophilic FPPS inhibitors could be of interest in the context of the development of inhibitors that inhibit prenylation in Ras-bearing tumors,[21] and the availability of structural data may help guide future lead development. Second, the structure of the TbFPPS complex with **8** is of interest because while all previously reported bisphosphonate−

FPPS structures contain a single bisphosphonate ligand, this complex, at least in the crystalline solid state, contains two, again as shown in the superposition in Figure 5, and **8** is a potential lead for selective *T. brucei* cell growth inhibitors. Overall, the results reported here are thus of general interest since they describe two new structures of FPPS—inhibitor complexes, of potential use in the design of new drug leads.

■ ASSOCIATED CONTENT

Ⓢ Supporting Information

Experimental details of human FPPS and TbFPPS expression, purification, and X-ray crystallography, together with a comparison of the apo and ligand bound TbFPPS structures and ligand interactions. This material is available free of charge via the Internet at http://pubs.acs.org.

■ AUTHOR INFORMATION

Corresponding Author

*E-mail: eoldfiel@illinois.edu.

Notes

The authors declare no competing financial interest.

■ ABBREVIATIONS

FPPS, farnesyl diphosphate synthase; IPP, isopentenyl diphosphate; DMAPP, dimethylallyl diphosphate; GPP, geranyl diphosphate; FPP, farnesyl diphosphate; ITC, isothermal titration calorimetry

■ REFERENCES

(1) Russell, R. G. Bisphosphonates: the first 40 years. *Bone* **2011**, *49*, 2−19.

(2) Martin, M. B.; Arnold, W.; Heath, H. T., 3rd; Urbina, J. A.; Oldfield, E. Nitrogen-containing bisphosphonates as carbocation transition state analogs for isoprenoid biosynthesis. *Biochem. Biophys. Res. Commun.* **1999**, *263*, 754−758.

(3) Bergstrom, J. D.; Bostedor, R. G.; Masarachia, P. J.; Reszka, A. A.; Rodan, G. Alendronate is a specific, nanomolar inhibitor of farnesyl diphosphate synthase. *Arch. Biochem. Biophys.* **2000**, *373*, 231−241.

(4) Boissier, S.; Ferreras, M.; Peyruchaud, O.; Magnetto, S.; Ebetino, F. H.; Colombel, M.; Delmas, P.; Delaisse, J. M.; Clezardin, P. Bisphosphonates inhibit breast and prostate carcinoma cell invasion, an early event in the formation of bone metastases. *Cancer Res.* **2000**, *60*, 2949−2954.

(5) Kunzmann, V.; Bauer, E.; Wilhelm, M. Gamma/delta T-cell stimulation by pamidronate. *N. Engl. J. Med.* **1999**, *340*, 737−738.

(6) Tsagozis, P.; Eriksson, F.; Pisa, P. Zoledronic acid modulates antitumoral responses of prostate cancer-tumor associated macrophages. *Cancer Immunol. Immunother.* **2008**, *57*, 1451−1459.

(7) Rodriguez, N.; Bailey, B. N.; Martin, M. B.; Oldfield, E.; Urbina, J. A.; Docampo, R. Radical cure of experimental cutaneous leishmaniasis by the bisphosphonate pamidronate. *J. Infect. Dis.* **2002**, *186*, 138−140.

(8) No, J. H.; de Macedo Dossin, F.; Zhang, Y.; Liu, Y. L.; Zhu, W.; Feng, X.; Yoo, J. A.; Lee, E.; Wang, K.; Hui, R.; Freitas-Junior, L. H.; Oldfield, E. Lipophilic analogs of zoledronate and risedronate inhibit *Plasmodium* geranylgeranyl diphosphate synthase (GGPPS) and exhibit potent antimalarial activity. *Proc. Natl. Acad. Sci. U.S.A.* **2012**, *109*, 4058−4063.

(9) Oldfield, E. Targeting isoprenoid biosynthesis for drug discovery: bench to bedside. *Acc. Chem. Res.* **2010**, *43*, 1216−1226.

(10) Oldfield, E.; Lin, F. Y. Terpene biosynthesis: modularity rules. *Angew. Chem., Int. Ed.* **2012**, *51*, 1124−1137.

(11) Liu, C. I.; Liu, G. Y.; Song, Y.; Yin, F.; Hensler, M. E.; Jeng, W. Y.; Nizet, V.; Wang, A. H.; Oldfield, E. A cholesterol biosynthesis inhibitor blocks *Staphylococcus aureus* virulence. *Science* **2008**, *319*, 1391−1394.

(12) Swiezewska, E.; Danikiewicz, W. Polyisoprenoids: structure, biosynthesis and function. *Prog. Lipid Res.* **2005**, *44*, 235−258.

(13) Jahnke, W.; Rondeau, J. M.; Cotesta, S.; Marzinzik, A.; Pelle, X.; Geiser, M.; Strauss, A.; Gotte, M.; Bitsch, F.; Hemmig, R.; Henry, C.; Lehmann, S.; Glickman, J. F.; Roddy, T. P.; Stout, S. J.; Green, J. R. Allosteric non-bisphosphonate FPPS inhibitors identified by fragment-based discovery. *Nat. Chem. Biol.* **2010**, *6*, 660−666.

(14) Amstutz, R.; Bold, G.; Cotesta, S.; Jahnke, W.; Marzinzik, A.; Mueller-Hartwieg, C.; Ofner, S.; Stauffer, F.; Zimmermann, J. Quinolines as inhibitors of farnesyl pyrophosphate synthase. U.S. Patent Application PCT/EP2009/052314, September 3, 2009.

(15) Ebetino, F. H.; Roze, C. N.; McKenna, C. E.; Barnett, B. L.; Dunford, J. E.; Russell, R. G. G.; Mieling, G. E.; Rogers, M. J. Molecular interactions of nitrogen-containing bisphosphonates within farnesyl diphosphate synthase. *J. Org. Chem.* **2005**, *690*, 2679−2687.

(16) Martin, M. B.; Grimley, J. S.; Lewis, J. C.; Heath, H. T., 3rd; Bailey, B. N.; Kendrick, H.; Yardley, V.; Caldera, A.; Lira, R.; Urbina, J. A.; Moreno, S. N.; Docampo, R.; Croft, S. L.; Oldfield, E. Bisphosphonates inhibit the growth of *Trypanosoma brucei, Trypanosoma cruzi, Leishmania donovani, Toxoplasma gondii*, and *Plasmodium falciparum*: a potential route to chemotherapy. *J. Med. Chem.* **2001**, *44*, 909−916.

(17) Poulter, C. D.; Satterwhite, D. M. Mechanism of the prenyl-transfer reaction. Studies with (E)- and (Z)-3-trifluoromethyl-2-buten-1-yl pyrophosphate. *Biochemistry* **1977**, *16*, 5470−5478.

(18) Aaron, J. A.; Christianson, D. W. Trinuclear metal clusters in catalysis by terpenoid synthases. *Pure Appl. Chem.* **2010**, *82*, 1585−1597.

(19) Liu, Y. L.; Lindert, S.; Zhu, W.; Wang, K.; McCammon, J. A.; Oldfield, E. Taxodione and arenarone inhibit farnesyl diphosphate synthase by binding to the isopentenyl diphosphate site. *Proc. Natl. Acad. Sci. U.S.A.* **2014**, *111*, E2530−E2539.

(20) Lindert, S.; Zhu, W.; Liu, Y. L.; Pang, R.; Oldfield, E.; McCammon, J. A. Farnesyl diphosphate synthase inhibitors from *in silico* screening. *Chem. Biol. Drug Des.* **2013**, *81*, 742−748.

(21) Xia, Y.; Liu, Y. L.; Xie, Y.; Zhu, W.; Guerra, F.; Shen, S.; Yeddula, N.; Fischer, W.; Low, W.; Zhou, X.; Zhang, H. Y.; Oldfield, E.; Verma, I. M. A combination therapy for KRAS-driven lung adenocarcinomas using liphophilic bisphosphonates and rapamycin. *Sci. Transl. Med.* **2014**, *6*, 263ra161.

(22) Tarshis, L. C.; Yan, M.; Poulter, C. D.; Sacchettini, J. C. Crystal structure of recombinant farnesyl diphosphate synthase at 2.6-A resolution. *Biochemistry* **1994**, *33*, 10871−10877.

(23) Hosfield, D. J.; Zhang, Y.; Dougan, D. R.; Broun, A.; Tari, L. W.; Swanson, R. V.; Finn, J. Structural basis for bisphosphonate-mediated inhibition of isoprenoid biosynthesis. *J. Biol. Chem.* **2004**, *279*, 8526−8529.

(24) Rondeau, J. M.; Bitsch, F.; Bourgier, E.; Geiser, M.; Hemmig, R.; Kroemer, M.; Lehmann, S.; Ramage, P.; Rieffel, S.; Strauss, A.; Green, J. R.; Jahnke, W. Structural basis for the exceptional *in vivo* efficacy of bisphosphonate drugs. *ChemMedChem* **2006**, *1*, 267−273.

(25) Kavanagh, K. L.; Guo, K.; Dunford, J. E.; Wu, X.; Knapp, S.; Ebetino, F. H.; Rogers, M. J.; Russell, R. G.; Oppermann, U. The molecular mechanism of nitrogen-containing bisphosphonates as

antiosteoporosis drugs. *Proc. Natl. Acad. Sci. U.S.A.* **2006**, *103*, 7829–7834.

(26) *Molecular Operating Environment (MOE)*, 2013.08; Chemical Computing Group Inc.: Montreal, Canada, 2014.

(27) Dunford, J. E.; Thompson, K.; Coxon, F. P.; Luckman, S. P.; Hahn, F. M.; Poulter, C. D.; Ebetino, F. H.; Rogers, M. J. Structure-activity relationships for inhibition of farnesyl diphosphate synthase in vitro and inhibition of bone resorption in vivo by nitrogen-containing bisphosphonates. *J. Pharmacol. Exp. Ther.* **2001**, *296*, 235–242.